Monthly Notices of the ROYAL ASTRONOMICAL SOCIETY

MNRAS **469,** S252–S261 (2017) doi:10.1093/mnras/stx1491
Advance Access publication 2017 June 21

Evolution of the ion environment of comet 67P during the *Rosetta* mission as seen by RPC-ICA

Hans Nilsson,[1,2]★ Gabriella Stenberg Wieser,[1] Etienne Behar,[1,2] Herbert Gunell,[3,4] Martin Wieser,[1] Marina Galand,[5] Cyril Simon Wedlund,[6] Markku Alho,[7] Charlotte Goetz,[8] Masatoshi Yamauchi,[1] Pierre Henri,[9] Elias Odelstad[10] and Erik Vigren[10]

[1]*Swedish Institute of Space Physics, Box 812, SE-981 28 Kiruna, Sweden*
[2]*Department of Computer Science, Electrical and Space Engineering, Luleå University of Technology, SE-981 28 Kiruna, Sweden*
[3]*Royal Belgian Institute for Space Aeronomy, Avenue Circulaire 3, B-1180 Brussels, Belgium*
[4]*Department of Physics, Umeå University, SE-901 87 Umeå, Sweden*
[5]*Department of Physics, Imperial College London, Prince Consort Road, London SW7 2AZ, UK*
[6]*Department of Physics, University of Oslo, PO Box 1048 Blindern, N-0316 Oslo, Norway*
[7]*Department of Electronics and Nanoengineering, School of Electrical Engineering, Aalto University, PO Box 15500, FI-00076 Aalto, Finland*
[8]*Institut für Geophysik und extraterrestrische Physik, Technische Universität Braunschweig, Mendelssohnstr 3, D-38106 Braunschweig, Germany*
[9]*LPC2E-CNRS, 3A avenue de la Recherche Scientifique, F-45071 Orléans, Cedex, 2, Orléans, France*
[10]*Swedish Institute of Space Physics, Box 537, SE-751 21 Uppsala, Sweden*

Accepted 2017 June 12. Received 2017 June 12; in original form 2017 April 5

ABSTRACT

Rosetta has followed comet 67P from low activity at more than 3.6 au heliocentric distance to high activity at perihelion (1.24 au) and then out again. We provide a general overview of the evolution of the dynamic ion environment using data from the RPC-ICA ion spectrometer. We discuss where *Rosetta* was located within the evolving comet magnetosphere. For the initial observations, the solar wind permeated all of the coma. In 2015 mid-April, the solar wind started to disappear from the observation region, to re-appear again in 2015 December. Low-energy cometary ions were seen at first when *Rosetta* was about 100 km from the nucleus at 3.6 au, and soon after consistently throughout the mission except during the excursions to farther distances from the comet. The observed flux of low-energy ions was relatively constant due to *Rosetta*'s orbit changing with comet activity. Accelerated cometary ions, moving mainly in the antisunward direction gradually became more common as comet activity increased. These accelerated cometary ions kept being observed also after the solar wind disappeared from the location of *Rosetta*, with somewhat higher fluxes further away from the nucleus. Around perihelion, when *Rosetta* was relatively deep within the comet magnetosphere, the fluxes of accelerated cometary ions decreased, as did their maximum energy. The disappearance of more energetic cometary ions at close distance during high activity is suggested to be due to a flow pattern where these ions flow around the obstacle of the denser coma or due to charge exchange losses.

Key words: plasmas – methods: data analysis – comets: individual: 67P.

1 INTRODUCTION

A comet atmosphere is not retained by the low gravity of the comet nucleus. The atmosphere expands into space surrounding the comet nucleus. The level of outgassing, the comet activity, is primarily governed by the insolation. The comet atmosphere is therefore very dynamic, continuously changing in size and density as the nucleus moves closer and further away from the sun.

As constituents of the comet atmosphere get ionized, by solar EUV, charge exchange reactions and particle impact ionization (Galand et al. 2016; Simon Wedlund et al. 2017), they affect and are affected by the magnetic and electric fields in the vicinity of the comet, i.e. the fields of the surrounding solar wind. The character of this interaction varies strongly with the comet activity. The most basic process that occurs is known as 'pick-up' of the cometary

★ E-mail: hans.nilsson@irf.se

ions. As the newly born cometary ions are accelerated by the solar wind convective electric field, they are picked up by the solar wind stream (Szegö et al. 2000). This is followed by a large-scale gyration of the newly picked up ions in the magnetic field of the solar wind (Richardson et al. 1987; Coates et al. 1989). This picture is valid when the solar wind is itself not too strongly affected by the presence of the comet atmosphere, i.e. at low activity or at large distances from the comet nucleus.

For the case of very high activity, with a large comet atmosphere, additional features occur in the solar wind–comet atmosphere interaction. A bow shock forms on the sunward side of the comet, as well as a cometary magnetopause through which the solar wind particles do not penetrate, as observed around 1P/Halley by Giotto (Cravens & Gombosi 2004). Close enough to the nucleus a diamagnetic cavity has been observed to form, into which the solar wind magnetic field does not penetrate. The case of high-activity large-scale comet atmospheres has been sampled by several missions, in particular at comet 1P/Halley (Neugebauer 1990).

The *Rosetta* mission (Glassmeier et al. 2007) provided the first opportunity to study the gradual evolution of comet atmosphere–solar wind interaction, from the small atmosphere of a low-activity comet at a heliocentric distance of more than 3.6 au, to a relatively more active comet at perihelion. The outgassing rate of *Rosetta*'s target comet, 67P/Churyumov Gerasimenko (hereafter 67P), changed from less than 10^{26} molecules s^{-1} upon *Rosetta*'s arrival in 2014 August, when the comet was about 3.6 au from the Sun, to 3.5×10^{28} molecules s^{-1} at a perihelion distance of 1.24 au reached on 2015 August 13 (Hansen et al. 2016). This can be compared to the estimated outgassing rate of comet 1P/Halley upon the Giotto encounter of about 10^{30} molecules s^{-1} (Krankowsky et al. 1986; Rème 1991). The outgassing rate of comet 67P at perihelion was rather close to that of comet 21P/Giacobini–Zinner during the ICE spacecraft encounter (Mendis, Houpis & Marconi 1985) and comet 19P/Borrelly during the DS1 spacecraft encounter (Young et al. 2004), and a few times more than that of comet 26P/Grigg–Skjellerup during the Giotto encounter (Johnstone et al. 1993). The observations made by *Rosetta* in the time from the rendezvous leading up to perihelion thus represent a unique parameter space as compared to all previous comet encounters.

The first clear signatures of plasma originating from comet 67P were detected in 2014 August, when *Rosetta* was at 100 km distance from the nucleus, using the *Rosetta* Plasma Consortium Ion Composition Analyser (RPC-ICA) and RPC-IES ion sensors (Edberg et al. 2015; Goldstein et al. 2015; Nilsson et al. 2015a). The first detected cometary ions were moving perpendicular to the solar wind flow direction, along the solar wind electric field. This can be expected for ionized particles in an undisturbed solar wind once they have gained some energy, which was needed for the initial detection of very faint fluxes. Due to conservation of momentum, once significant amounts of cometary ions become accelerated by the solar wind electric field, the solar wind is deflected in the direction opposite to the solar wind electric field (Broiles et al. 2015; Behar et al. 2016a). The solar wind deflection in the vicinity of comet 67P was observed to gradually increase with the comet activity (Behar et al. 2016b), reaching nearly 90° at an heliocentric distance of 2.2 au, while very little slowing down of the solar wind was observed. The neutral atmosphere directly interacted with the solar wind stream through charge exchange reactions, visible through the presence of He^+ ions resulting from charge exchange of He^{2+} with the comet atmosphere (Nilsson et al. 2015a; Simon Wedlund et al. 2016), and even H^- resulting from double charge exchange (Burch et al. 2015). During the same period, the magnetic field magnitude in the vicinity of the comet increased from about 5 nT to about 25 nT (Behar et al. 2016b; Goetz et al. 2017). The main magnetic field signature observed during initial observations was a strong wave activity at about 40 mHz with a wave amplitude similar to the background level, known as 'the singing comet' (Richter et al. 2015).

The cold plasma of cometary origin dominated the local ion density more or less from the start of *Rosetta* observations as revealed by the RPC-LAP Langmuir probe and RPC-MIP mutual impedance probe instruments. Initially observed densities ranged from a few ions per cm^3, i.e. similar to the solar wind, gradually increasing with time, reaching a density of about 100 cm^{-3} at 10 km distance from the nucleus and 3.1 au from the Sun (Edberg et al. 2015). The ion density was shown to fall off with distance r from the nucleus as $1/r$ (Edberg et al. 2015) for these conditions. The spacecraft potential during the same part of the mission was typically negative, reflecting that the electrons had not been much cooled by collisions (Odelstad et al. 2015). These warm electrons of energy 5–10 eV were present persistently throughout the mission, interspersed with filaments of very cold electrons with a temperature of less than 0.1 eV (Eriksson et al. 2017). The cold electrons observed around perihelion are believed to have been cooled by collisions with neutrals in the denser part of the coma.

Both plasma and neutral gas observations also showed strong variations with comet rotation and summer/winter hemisphere (Bieler et al. 2015; Edberg et al. 2015; Goldstein et al. 2015; Hässig et al. 2015; Luspay-Kuti et al. 2015; Odelstad et al. 2015; Galand et al. 2016; Yang et al. 2016). Outgassing rate and plasma density were highest when the neck region of the comet was sunlit, and over the summer hemisphere during the inbound leg of the comet orbit.

The electron environment of comet 67P was also investigated using the RPC-IES ion and electron sensor. Clark et al. (2015) reported electrons accelerated up to about 100 eV. Broiles et al. (2016a) fitted two electron populations with kappa distributions to the observations at low activity (2014 October 30) and near perihelion (2015 August 15) and reported one dense and warm population (10 cm^{-3}, 2×10^5 K) and one hot and rarefied population (0.005 cm^{-3}, 5×10^5 K). They concluded that the former was of cometary origin and the latter, the solar wind halo electrons. Madanian et al. (2016) used a two-stream electron transport code to interpret the IES data, noting that the fluxes in the 5–200 eV range could not be explained by their model. Such high-energy electrons strongly affect the spacecraft potential (Odelstad et al. 2015) as well as ambipolar diffusion of the ions (Vigren & Eriksson 2017) and affect impact ionization. Galand et al. (2016) assessed the contribution of the ionization sources for the case of low activity during pre-perihelion, showing that solar EUV drove ionization over the summer (north) hemisphere, whereas electron-impact ionization was needed to explain the electron densities in the winter hemisphere, sometimes reaching values higher than on the summer hemisphere. How the cometary electrons are heated is unclear, but Karlsson et al. (2017) suggested that lower hybrid waves observed using the RPC-LAP instrument may cause the observed warm electron populations. Broiles et al. (2016b) reached a similar conclusion based on the RPC-IES data.

In addition to the cold ion population, a population of accelerated cometary ions became more common, more intense and reached higher energies as activity increased. The flow direction of these accelerated ions turned out to be mainly antisunward (Nilsson et al. 2015b). Given that the gyro radius of newly picked up ions was of the order of 10 000 km during the initial part of the mission, this was in clear contradiction to basic expectations. It has been suggested that this antisunward flow could be due to a polarization electric field arising due to different motion of newly created cometary

ions and electrons under the influence of the solar wind electric field (Nilsson et al. 2015b; Behar et al. 2016a). Detailed studies of energy-angle dispersion of accelerated cometary ions indicate that part of the observations can be explained through a smaller gyroradius of the observed cometary ions than what is expected for the observed magnetic field and assumed solar wind electric field (Nicolaou et al. 2017). This would be consistent with a polarization electric field partially shielding the solar wind electric field, but could possibly also be explained through magnetic field draping. Other ion energy dispersion events are not consistent with a gyromotion, so the situation is rather complex.

As cometary activity increased further, the solar wind disappeared from the location of *Rosetta* in 2015 late-April (Mandt et al. 2016; Behar et al. 2017), a solar wind cavity had formed around the comet. Inside this comet magnetosphere, a further plasma boundary was observed with higher energy ions seen outside the boundary, while lower energy ions, reduced magnetic field pile up and enhanced electron densities were seen inside of the boundary (Mandt et al. 2016). The boundary was suggested to be related to ion-neutral collisions with a change in ion composition inside compared with outside (Fuselier et al. 2016). A diamagnetic cavity was also frequently observed between 2015 April 20 and 2016 February 17 (Goetz et al. 2016a,b; Nemeth et al. 2016). This diamagnetic cavity appears related to an inner region where electrons are collisionally coupled to the neutral atmosphere, and the *Rosetta* observations were likely made in filaments of plasma extending from this inner region (Henri et al. 2017).

We complement these previous studies by showing the evolution of the ion environment, as seen by the RPC-ICA instrument, from arrival at the comet in 2014 August to the end of the *Rosetta* mission in 2016 September. The main purpose is to provide a context for the many more detailed studies yet to come.

2 METHODS

2.1 Instrument description

This study is based on data from the RPC-ICA, an ion spectrometer with modest mass resolution capabilities (Nilsson et al. 2007). The energy range of the instrument is from a few eV up to 40 keV per elementary charge (e) for positively charged ions, with an energy resolution of 7 per cent. RPC-ICA can distinguish between mass groups of 1, 2, 4, 8, 16 and 32 amu e^{-1}. A post-acceleration voltage is used after the electrostatic analyser, and this affects the mass range and mass resolution of the instrument. Incoming ions are detected by 16 directional anodes (sectors) and 32 mass anodes (mass channels).

The instrument performs a full energy sweep of 96 energy steps in 12 s, with an acquisition time per energy level of 120.9 ms. A near 2.8π sr field of view is achieved through electrostatic entrance deflection in 16 steps, taking 192 s. The practical field of view is about 2π sr due to spacecraft shadowing. The angular coverage is worse at low energy (below about 100 eV) and at energies above 15 keV. The angular resolution is $22.5 \times 4^{\circ}$ at maximum resolution. To stay within available telemetry limits, the data were sometimes binned onboard to a coarser angular resolution. We refer the reader to Nilsson et al. (2007) for further details on the instrument and its modes, and to Nilsson et al. (2015b) for a discussion of a number of instrument limitations discovered *in situ*.

Whereas we do not report data from any other *Rosetta* Plasma Consortium (Carr et al. 2007) instruments in this paper, we have throughout our analysis of RPC-ICA data made use of RPC-LAP Langmuir probe estimates of the spacecraft potential (Eriksson et al. 2007), magnetic field data from RPC-MAG (Glassmeier et al. 2007) as well as ion data from RPC-IES Ion and Electron Sensor (Burch et al. 2007).

2.2 Data handling

The aim of this study is to present a broad overview of the ions of solar wind and cometary origin in the energy range covered by the RPC-ICA instrument. We have therefore selected to use a relatively uniform data set, using only data that cover the full energy range of the instrument. To have suitable coverage of the solar wind protons, we only use data with high post-acceleration. This still corresponds to a vast majority of the full data set.

The data are typically rather clean, but some noise exists. In particular, noise increased with insolation. For each energy scan, we have therefore subtracted the median of the counts (per acquisition cycle of 120.9 ms) of all energy channels to remove enhanced background that is energy independent. This was done independently for each directional and mass anode. After signals from different mass anodes were added to form physical mass ranges, any data with a negative value were set to 0.

To make loss-less compression more efficient, a noise reducing background subtraction was frequently used on board. Typically two counts were subtracted from all data points (at each energy level, mass and direction anode). The background subtraction was performed after onboard binning, so the average reduction per measurement point varied with binning as well. To make the data set uniform, we have adjusted the data, setting all individual data points less than two to zero. We have then compensated data points with more than four counts for the background subtraction performed onboard, adding as much as was subtracted.

Data were binned into two mass ranges: water group ions and heavier, and helium ions and lighter. Sometimes there is electronic cross-talk with a strong signal in one mass range spilling over to the other mass range. This is rather easily detectable by manual inspection. For this paper, we have set the data in the mass range with a weaker signal to zero for all data. This is done individually for each energy level, and as typically solar wind and cometary ions are seen in different energy ranges and coming from different directions, this affects only a small part of the data.

Calculations of flow directions in terms of cone angle (to be further defined below) were done at full temporal resolution, as were calculations of moments. In order to show the data for the whole mission, the data were then averaged over 1 h or more.

2.2.1 Energy table

As discussed in Nilsson et al. (2015a), it was discovered upon arrival at comet 67P that the RPC-ICA high voltage had an offset of more than 33 V as compared to laboratory calibration results. This resulted in an offset of the energy table of more than 300 eV, and ions measured at a nominal energy of 300 eV according to the original energy table had an actual energy close to zero. Using *in situ* housekeeping data of the actual high voltage values and by analysing observed particles distributions, the exact voltage could be determined to within a level of about 1 V. The analyser constant of ICA is about 10, so the resulting uncertainty of the exact energy level of detected ions was about 10 eV. Indeed, some case studies indicated that the initial new estimates of the energy levels used for example in Nilsson et al. (2015b) were about 10 eV too high (Gunell et al. 2017). Comparison with spacecraft potential estimates

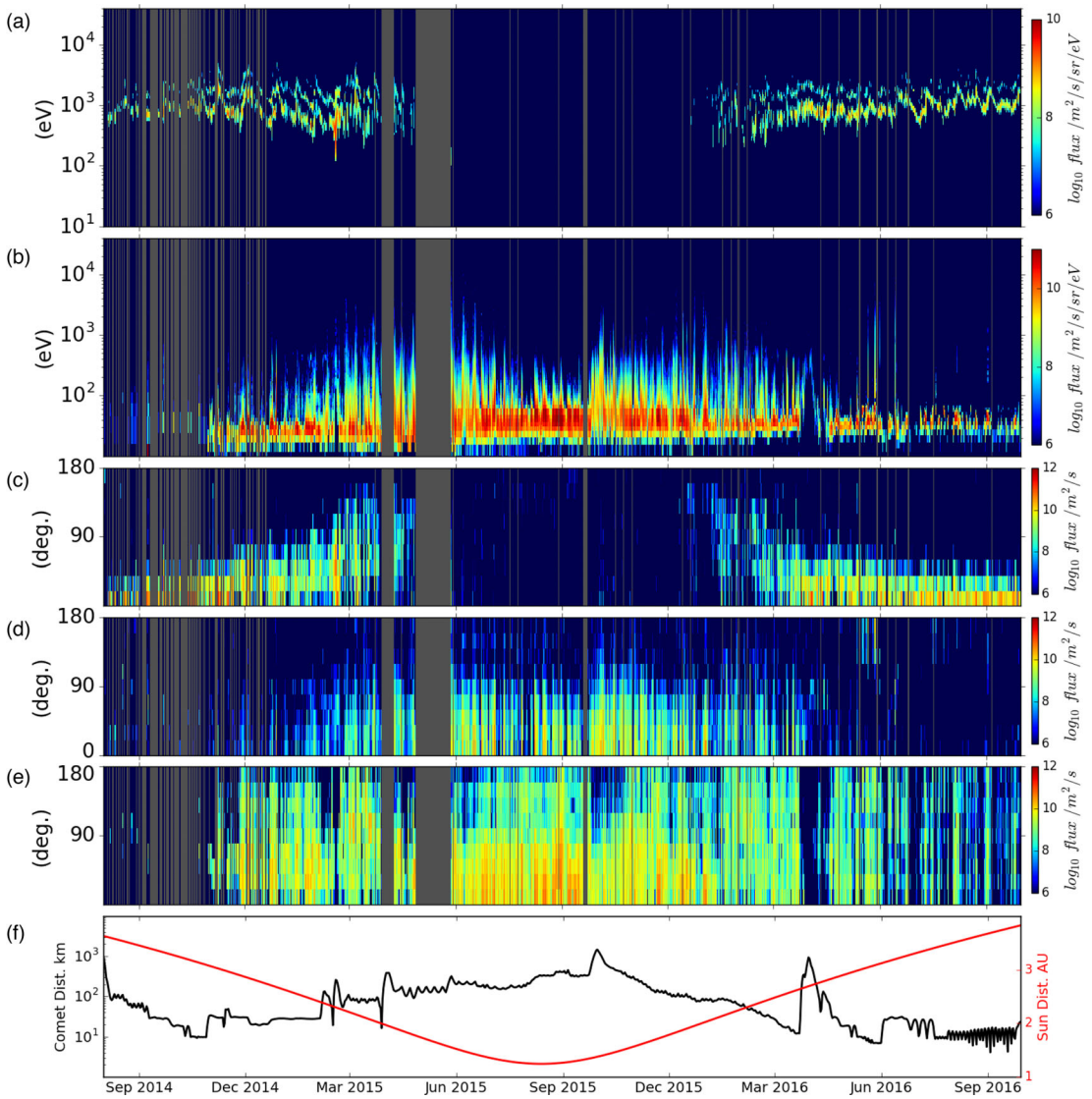

Figure 1. Energy spectrograms summed over all viewing directions and integrated over 1 h for (a) solar wind ions and (b) cometary ions (m^{-2} s^{-1} sr^{-1} eV^{-1}). The *y*-axis shows energy per charge (eV e^{-1}). Panels (c)–(e) show the integrated flux (m^{-2} s^{-1}) of ions as function of cone angle for solar wind ions (c), and for cometary ions in the energy ranges above 100 eV (d) and below 60 eV (e). 0° cone angle corresponds to antisunward flow. Panel (f) shows the heliocentric distance [red line, right *y*-axis (au)] and the distance to the comet [black line, left *y*-axis (km), note the logarithmic scale].

from the RPC-LAP Langmuir probe confirmed this and allowed us to further improve the correction (Odelstad et al. 2017). The remaining uncertainty of the current best energy level estimate is about 3 eV.

The offset correction made the energy steps of the original energy table sparse, and the elevation deflection voltage out of sync with the energy level, yielding also poor angular coverage at energies below about 100 eV. Improved tables were uploaded to RPC-ICA on several occasions, first on 2014 October 30. Angular coverage is still poorer below 100 eV than above also after the updated tables, due to insufficient accuracy of the voltages controlling the elevation deflection.

Apart from this remaining uncertainty, there is a temperature-related drift of the high voltage, which to a first approximation can be corrected with the formula:

$$E_c = \begin{cases} E_0 + (13.5 - T_s) \times 0.7, & \text{when} \quad T_s < 13.5\,^{\circ}\text{C} \\ E_0, & \text{otherwise} \end{cases}, \qquad (1)$$

where E_0 is the nominal energy level in eV and T_s, the sensor temperature in °C. The most severely affected period was 2015 April, when the instrument at times became very cold. After 2015 May the temperature regulation of the instrument was adjusted to stay within a narrower temperature interval.

The energy of the observed ions is also affected by the spacecraft potential, which can be estimated using RPC-LAP. We have not attempted to compensate for the spacecraft potential in this work. When *Rosetta* is close to the nucleus, the lower border of significant counts in the RPC-ICA data typically corresponds to the spacecraft potential but with an as yet not finally determined offset. Also with the low temporal resolution of Fig. 1(b), the cometary ion spectra frequently have a lower border at 10–30 eV, corresponding to spacecraft potentials in the range −10 to −30 eV.

The lowest energy detectable by RPC-ICA is currently believed to be a few eV, determined from the lower border of the cometary ion spectra for periods with negative spacecraft potential and observations made close to the nucleus (Odelstad et al. 2017). This is

significantly less than the value of 25 eV given in the instrument paper. The high value in the instrument paper was determined from laboratory estimates of the voltages on both the electrostatic analyser and the entrance deflection plates. As noted earlier, there was in practice a large offset between these results and *in situ* results. One may also note that the ASPERA-3 Ion Mass Analyser on Mars Express, nearly identical to RPC-ICA, has a similar low-energy range of a few eV as is the current best estimate for RPC-ICA.

2.2.2 *Flow angle calculation*

It was noted in Nilsson et al. (2015b) and Behar et al. (2016a) that the antisunward component was dominating the flow direction of cometary ions. We investigate this further by looking at the total flux for different angles with respect to the antisunward direction. We term this angle the *cone angle*, see Behar et al. (2016a, 2017) for illustrations and further discussion. We define the cone angle as 0° in the antisunward direction, and thus a 180° cone angle represents the flow in the sunward direction. Data were binned into 20°-wide bins. The total physical flux in each energy bin was calculated and assigned to a cone angle bin. The resulting data were then averaged for each bin and energy level. Finally, the flux was summed over energy bins.

The spacecraft blocks part of the RPC-ICA field of view. The most common observational geometry is a nadir-pointing terminator orbit, in which case RPC-ICA has some unobstructed field of view both in the sunward direction and in the antisunward direction, see Behar et al. (2016a,b) for illustrations of actual examples. We therefore expect that our discussion of the cone angle of the flow is not strongly affected by the limited field of view.

2.2.3 *Data at low altitude*

From 2016 May, as *Rosetta* was going closer to the nucleus, RPC-ICA data contained a number of signals that are suspected to be instrumental artefacts. These include frequent detection of ions at energies below the spacecraft potential. In other cases, a signal was detected over a broad energy range, but this signal only occurred at low altitude. All these data are subject to further investigation. This suspicious data are included in the data shown in this study. At the level of detail we are dealing with, this mainly affects a high-energy cometary ion population moving sunward, seen in 2016 May. The suspicious low-energy population, which appear at energies below the energy corresponding to the spacecraft potential, is difficult to distinguish from just less negative spacecraft potential in the plot shown in this study. At high resolution, one can clearly see a separate population at energies below the main low-energy population.

3 OBSERVATIONS

3.1 Energy and angular distributions

RPC-ICA was run sparingly in the beginning of the mission due to instrument problems, i.e. from arrival at the comet in 2014 August until 2014 December. Moreover, a suspected high-voltage problem led to the use of a low-energy mode in most of 2015 May, data that are not included in this study. Fig. 1 shows an overview of all RPC-ICA data obtained from arrival at the comet (2014 August 1) to end of mission (2016 September 30). Grey intervals indicate time periods with no data. The uppermost panel (a) shows an energy spectrogram of solar wind ions, i.e. ions in the mass range 1–4 atomic mass units per charge (amu e^{-1}). The *x*-axis shows Universal Time, the *y*-axis energy per charge and the colour indicate $\log_{10}$ differential flux (ions m^{-2} s^{-1} eV^{-1} sr^{-1}). The second panel (b) shows the same for heavier ions, in practice of cometary origin, in the mass range 16 amu e^{-1} and above. During the full mission, this population was dominated by water ions (H_2O^+ and H_3O^+) (Fuselier et al. 2015, 2016) except in summer 2015 near perihelion when additional chemical pathways could take place and the terminal ion was observed to be NH_4^+ at times (Beth et al. 2016). The third panel (c) shows the average solar wind flux, binned into nine different cone angle bins 20° wide, with 0° corresponding to antisunward flow. The fourth panel (d) shows the total cometary ion flux for ions with an energy above 100 eV in the same way. The fifth panel (e) shows the same for cometary ions with an energy below 50 eV. The lowermost panel (f) shows the cometocentric distance (black line) and the heliocentric distance (red line). Perihelion for comet 67P occurred on 2015 August 13.

In the solar wind data, Fig. 1(a), two or three narrow lines can be seen in the energy spectrogram, corresponding to H^+, He^{2+} and He^+ ions of solar wind origin, all at close to the same speed. The He^+ ions result from charge exchange of He^{2+} with cometary neutrals. The ratio of He^+ to He^{2+} flux can be used to estimate the integrated coma density along the flight path of the solar wind ions (Hansen et al. 2016; Simon Wedlund et al. 2016). In late-April, the solar wind starts to disappear, only to re-appear again in 2015 December as *Rosetta* was on the outbound leg of its journey, past perihelion [see also Behar et al. (2017) for further details on the solar wind ions and the formation of the solar wind cavity]. We show the cone angle of the solar wind ions in panel (c) but refer the reader to Behar et al. (2017) for further details on the solar wind flow and its evolution during the mission.

In the cometary ion data (Fig. 1b), one can see that ions are present in the energy interval up to about 30 eV consistently from 2014 December and until the end of the mission, with the exception of the nightside excursion around the end of 2016 March. During the dayside excursion in 2015 September, a decrease in the lowest energy ions observed can be discerned, i.e. the energy spectra are lifted up somewhat in energy. From 2015 June to 2015 December, cometary ions are consistently present up to about 70 eV when looking at 1 h resolution. Note that the plot shows 1-h integrated data, so this may to a large extent represent temporal variability. High time resolution data are needed to fully characterize the width of the energy spectra (Stenberg Wieser et al. 2017). A cut-off can be discerned in the plot at about 70 eV. This corresponds to where RPC-ICA starts to get better elevation coverage. Below that energy, RPC-ICA covers a much smaller range of angles out of the detector symmetry plane (see Nilsson et al. 2007, for a description of the elevation coverage of RPC-ICA as function of energy). As the data show the average differential flux for all contributing data, this shows that the additional elevation coverage at higher energies contributes to a lower average differential flux, i.e. the flux is limited in its angular extent.

The spacecraft potential affects the lowest energy in the local plasma population that can be measured by RPC-ICA. When the spacecraft potential is low or positive it is likely that part of the population cannot reach the detector. It is also possible that the limited field of view of RPC-ICA plays a much larger role for the lowest energy ions when the spacecraft potential does not attract ions from all directions. A negative spacecraft potential will accelerate ions towards the spacecraft and thus make lower energy ions easier to measure. Much of the time, RPC-ICA does not detect any ions at the

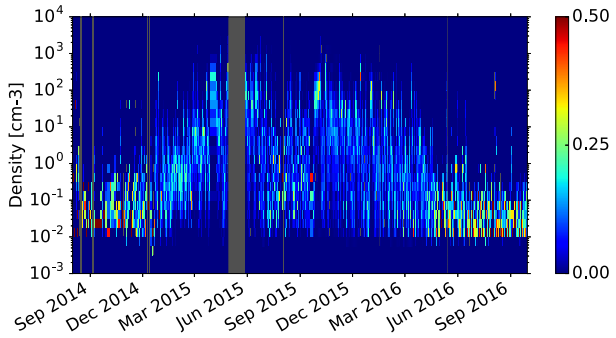

Figure 2. Daily colour-coded histograms of occurrence rate of different density estimates for cometary ions with an energy above 100 eV. We do not try to estimate the density from the RPC-ICA data at lower energy here, as the angular coverage is worse and effects of spacecraft potential and uncertainty in the precise energy scale matters at low energy. The *y*-axis shows the density (cm^{-3}), while the *x*-axis shows Universal Time.

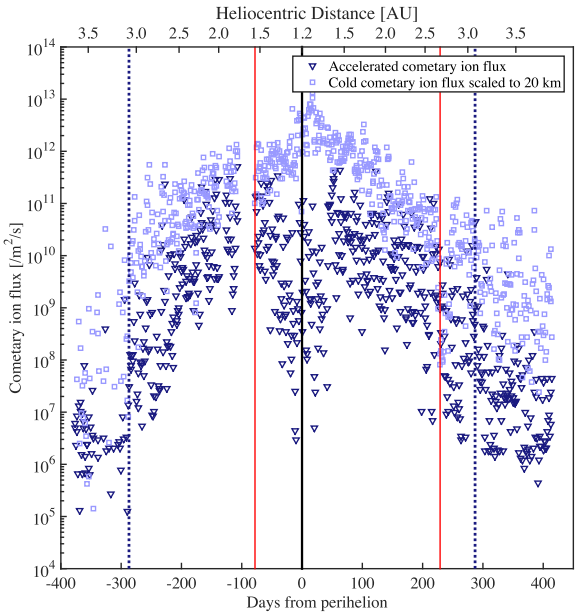

Figure 3. Accelerated water ion flux integrated over the energy interval 100–5 keV and over 24 h, as a function of time from perihelion (lower *x*-axis, days) and heliocentric distance (upper *x*-axis, au) are shown as dark blue triangles. For reference, we also show the total integrated cold water ion flux, scaled to 20 km comet distance assuming a r^{-1} fall-off with distance (light blue squares). Perihelion is indicated with a vertical solid black line. The time/distance when a change of RPC-ICA energy and elevation tables took place is indicated with a dotted blue line for the inbound leg and a corresponding line during the outbound leg. Red lines indicate equinoxes.

lowest energy levels, which is due to a negative spacecraft potential prevailing throughout most of the mission. Odelstad et al. (2017) reported the spacecraft potential for the period from 2014 September until end of mission. The spacecraft potential was mostly negative except for the period 2015 April to mid-June, the dayside excursion (2015 September) and the nightside excursion (2016 March). 2015 April to May coincides with a period when the RPC-ICA was very cold that affects the energy scale, but the fluxes in the lowest energy range seen in Fig. 1(b) for that time period is consistent with a positive spacecraft potential. During the excursions there was much less low-energy ions seen, which could be caused by the positive spacecraft potential preventing these ions from being observed. Case studies using high time resolution data shows that such energy spectra with no low-energy ions occur also for negative spacecraft potential (Stenberg Wieser et al. 2017). Thus, for much of the mission, we believe that the spacecraft potential does not strongly affect the fluxes we report here, though comparisons with the LAP and MIP instruments will be needed to elucidate how much of the real flux RPC-ICA picks up given constraints in energy range, angular range and the effect of the spacecraft potential.

The cone angle of the accelerated cometary ion fluxes is typically less than 90°, i.e. flowing in the antisunward direction. The ions at energies below 50 eV show a more even distribution of the cone angle of their flow. Around perihelion, when the spacecraft was at a relatively large distance from the nucleus, there is a tendency for the low-energy population to also drift in the antisunward direction. The flow direction of the low-energy ions may be strongly affected by the spacecraft potential. As *Rosetta* is typically nadir-pointing, flow at cone angles around 90° is typically away or towards the nucleus. Details of the flow in relation to the nucleus is the subject of a forthcoming more detailed study taking also the solar wind electric field direction into account.

3.2 Density of accelerated cometary ions

Fig. 2 shows the plasma density of cometary ions (mass per charge corresponding to water ions or heavier) with an energy of more than 100 eV as daily colour-coded histograms. The estimated densities were obtained through numerical integration of observed fluxes and assuming the mass to be that of water ions. No attempt to compensate for the limited field of view was made. The histograms are normalized to 1. As can be seen, densities were very low during the initial and final parts of the mission and also relatively low around perihelion. During periods with stronger accelerated cometary ion fluxes, the density sometimes reaches more than 100 cm^{-3} or one to two orders of magnitude more than the surrounding solar wind.

To illustrate how the ion flux varies with comet activity, we show the 24 h average flux of accelerated cometary ions (above 100 eV, dark blue triangles) and of cold ions (below 50 eV, light blue squares) in Fig. 3 as a function of days from perihelion (lower *x*-axis) and heliocentric distance (upper *x*-axis). Note that for all ions this is an integration of observed fluxes, which in particular at low energies may underestimate the total flux due to the limited field of view of the instrument. Perihelion is also indicated with a thick vertical black line. The 24-h average means that we integrate over about two cometary rotations, removing most of the longitudinal variability of the comet coma. As the energy scales were corrected on RPC-ICA on 2014 October 30, we have indicated that date/distance with a vertical dotted blue line. A similar line is shown for the same heliocentric distance in the post-perihelion data to allow for a comparison of the impact of the changed energy and elevation tables. As discussed in Nilsson et al. (2015b), we have tried to compensate for the changed tables when calculating the fluxes shown here. In general we can confirm the strong dependence of the average flux on the heliocentric distance, changing four orders of magnitude between 3.5 and 1.3 au. The accelerated cometary ion fluxes dip close to perihelion; this is seen clearly also in the energy spectrogram. We have scaled the cold cometary ion fluxes to a reference altitude of 20 km, assuming that the cold ion flux scale as $1/r$ with distance (Edberg et al. 2015; Nilsson et al. 2015b). For reference, we also show the equinoxes with red vertical lines. There is little change in the total flux connected to the changing seasons.

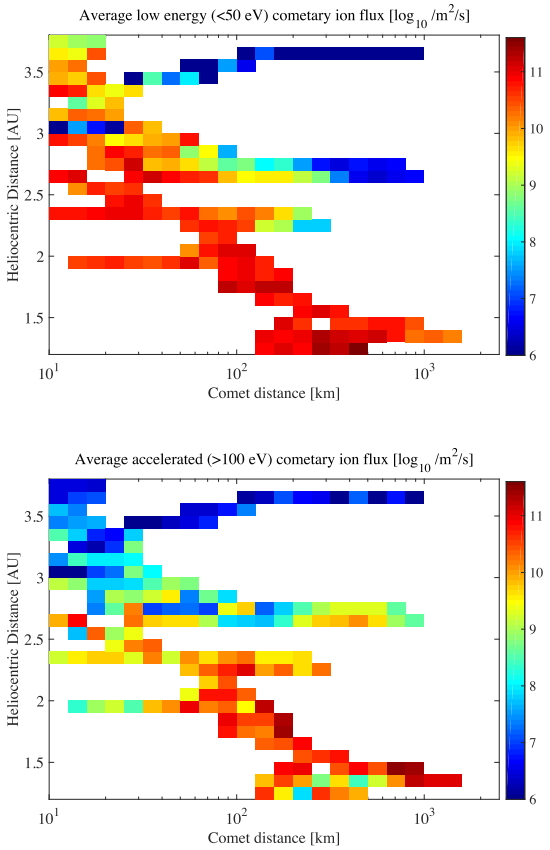

Figure 4. Average cold (top) and accelerated (bottom) cometary ion fluxes with respect to cometocentric distance (km) and heliocentric distance (au). *Rosetta*'s arrival at comet 67P in 2014 August, the nightside excursion, and the dayside excursion are clearly seen at 3.7, 2.7 and 1.3 au, respectively.

3.3 Spatial overview of the comet magnetosphere

Whereas *Rosetta* followed comet 67P over a large range of different cometary activity and made measurements at a large range of distances from the nucleus, the actual part of the activity/comet distance parameter space studied was rather narrow. We illustrate this in Fig. 4 where we show the average flux of cold cometary ions (upper panel) and accelerated cometary ions (lower panel) as function of the distance to the nucleus (x-axis) and the heliocentric distance (y-axis). Large cometocentric distances were covered in just a few events that stand out in Fig. 4: the comet approach in 2014 August (at 3.5–3.6 au), the dayside excursion in 2015 September at 1.4 au and the nightside excursion at 2.7 au. The close flyby followed by an excursion in 2015 late-February can also be clearly identified in Fig. 4.

One can see that the flux of cold ions is rather constant from perihelion up to about 3 au heliocentric distance, with the exceptions of the excursions further away from the nucleus. In particular, the nightside excursion at about 2.7 au stands out. This is clear also in the energy spectrogram, where the cold population is present essentially everywhere except during the tail excursion, the dayside excursion and during the approach phase in 2014 August. The cold ion flux falls off with distance from the nucleus and increases with decreasing heliocentric distance as can be expected. The rather constant flux for the lower energy ions is the result of *Rosetta* typically staying as close as possible to the nucleus. For operational reasons, this meant a similar atmospheric density throughout much of the mission.

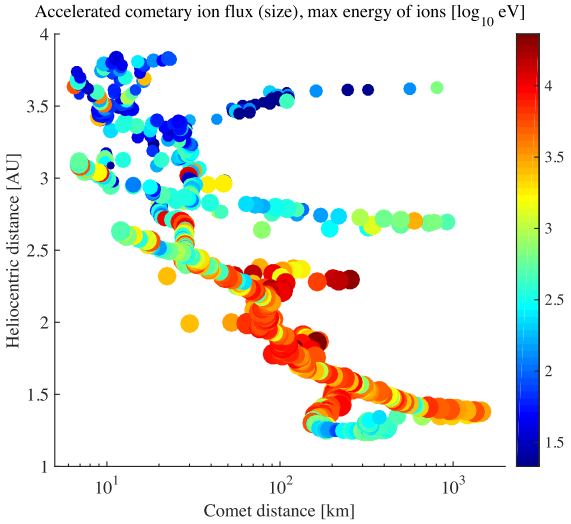

Figure 5. Magnetosphere overview: maximum energy of accelerated cometary ion fluxes with respect to heliocentric distance (au) and cometocentric distance (km). The size of the circles is proportional to the logarithm of the flux while the colour code indicates the $\log_{10}$ of the maximum energy (colour bar).

The accelerated ions show a somewhat different behaviour. There is a tendency towards higher fluxes further away from the comet nucleus, with the exception of large comet distances at large heliocentric distances, i.e. for low comet activity. We extend the look at accelerated cometary ions a bit further, by showing in Fig. 5 the maximum energy of cometary ions (with a flux in the energy bin $>10^8$ m^{-2} s^{-1}) observed during 24 h (colour code), as function of comet distance (x-axis) and heliocentric distance (y-axis). The average accelerated cometary ion flux is indicated with the size of the data points (being proportional to the logarithm of the flux). Each data point corresponds to 24 h of data. Here, a tendency can be seen with higher energy further away from the nucleus for heliocentric distances less than about 3 au. The maximum energy also increases closer to the Sun, with the exception of the region corresponding to the smallest heliocentric distances, where the ion energy and the ion flux drop. This could also be seen in the energy spectrograms, but it is even clearer how this region stands out in the data from this plot. The gradual increase of energy with comet distance is clearest for the tail excursion at around 2.7 au. There the energy increases in the flow direction, so the situation is clearly different as compared to the rest of the mission.

3.4 Discussion

At a first glance, the energy spectra shown in Fig. 1(a) and (b) bear similarities to the passage of a spacecraft through the magnetosheath and induced magnetospheres of Mars or Venus (Lundin et al. 2006; Martinecz et al. 2008). The passage of *Rosetta* through the different regions of comet 67P took more than 2 yr, and both the comet and the solar wind changed much during that time. The comet magnetosphere grew and encompassed *Rosetta* during a large part of the mission.

During low activity, the cometary coma is interacting with the solar wind that from the energy spectrograms looks rather undisturbed. The solar wind flow direction is much affected by the passage through the cometary coma, as discussed in detail in Behar et al. (2017). Around the disappearance of the solar wind from the

location of *Rosetta*, the energy spectra appear somewhat broadened towards lower energies, but there is very little change of energy. There is thus no classical bow shock or magnetosheath observed at that point. The strong deflection of the solar wind, where the solar wind ions appear to gyrate in the local magnetic field, can however be seen as a macroscopic slowing down of the bulk flow velocity. The gyromotion of the solar wind ions can be seen as corresponding to a transfer of energy from bulk velocity to thermal energy in a shock, as discussed in more detail in Behar et al. (2017).

Cometary ions, both cold and accelerated, dominate the plasma population around the comet long before the solar wind disappears from the position of *Rosetta*. The accelerated cometary ion fluxes generally increase with proximity to the Sun, except for the period closest to the Sun, 2015 July to 2015 September, when there is a minimum in accelerated cometary ion fluxes (Figs 1b, 4b) as well as a minimum in peak energy (Fig. 5). This corresponds to a period when *Rosetta* was relatively deep inside the comet magnetosphere and relatively far from the nucleus (at a few 100 km distance) and when the diamagnetic cavity was frequently observed (Goetz et al. 2016a).

The coldest and densest plasma is the component most difficult to study with RPC-ICA due to the limited field of view, the low-energy threshold of the instrument and the effect of a significant electric potential of the spacecraft. The rather wide angular spread of low-energy ions may be due to the spacecraft potential dominating over the ion bulk drift, attracting ions from all directions. A notable feature in the RPC-ICA data is the large energy interval covered by the continuously present colder population. In part this is due to a rapidly varying spacecraft potential (Odelstad et al. 2015; Odelstad et al. 2017). The energy spectra seen around perihelion typically have a width well above the acceleration given to the ions by the negative spacecraft potential. Frequently we see a width of about 60 eV around perihelion (reaching about 70 eV, see Fig. 1, but starting at 10–20 eV). Part of this width may be attributed to production of ions at different distance from the spacecraft in the presence of an electric field. Ions produced further away will then have passed through a larger potential drop and have acquired a higher energy when they reach the observation point.

Vigren & Eriksson (2017) examined the coupling of ions and neutrals using a one-dimensional model of water ions with acceleration by an ambipolar electric field interrupted by charge-exchange collisions. They found that these low-energy ions were typically decoupled from the motion of the neutral atmosphere. The width of their modelled energy spectra was 2–5 eV, which together with variations of the spacecraft potential may explain most of the energy spectra of the low-energy ions observed by RPC-ICA, but likely not all. Because of the role of the spacecraft potential, which can vary on short time-scales, we leave a closer examination for future work using high time resolution data (Stenberg Wieser et al. 2017).

Fluxes of accelerated cometary ions increased during the dayside excursion taking place between 2015 September 24 and October 8 (Edberg et al. 2016). This indicates that we have higher fluxes of the accelerated cometary ions further out in the comet magnetosphere. The low fluxes in 2015 July to September corresponds to when *Rosetta* was relatively deep inside the comet magnetosphere. This is also consistent with the findings of Mandt et al. (2016) who identified a boundary in the plasma data outside of which accelerated cometary ions were typically seen. They suggested the boundary to be related to the degree of collisions with neutral gas. The fluxes of cometary ions are consistently antisunward, so the boundary is not a feature frozen to the accelerated ions. So either there is plasma flow through the boundary, in which case the plasma changes its characteristics, i.e. lose energy due to collisions, or the precise flow of the energetic ions is around the boundary.

Estimates from Mandt et al. (2016) indicate that *Rosetta* is typically close to the ion collisionopause, defined as the region where the ion mean free path is equal to the distance to the nucleus. The distance to the nucleus is a characteristic length-scale of the cometary ionosphere (Galand et al. 2016). Outside of the collisionopause, most ions will experience less than one collision. As *Rosetta* was located close to the collisionopause, collisions are likely to have some effect. When charge-exchange collisions dominate, a single such collision is enough to remove an energetic ion and turn it into a cold ion. Therefore, the rather low neutral densities outside of the location of *Rosetta* may be able to explain the lower fluxes, though this needs to be modelled to assess how the energy spectra would change with distance as ions enter a progressively denser atmosphere. Another possible explanation for the behaviour of the accelerated cometary ions is that there is more acceleration of cometary ions further out in the magnetosphere, closer to the source of energy that is the solar wind. These accelerated ions do not reach the inner part of the magnetosphere due to their flight trajectories, they go around the obstacle of the inner part of the magnetosphere. These ions do have a consistent antisunward flow, but the cone angle is spread over a rather wide range of values between 0° and 90°. It is also possible that the peak energy of the water ions becomes lower if the amount of water ions increases faster than the available energy from the solar wind. A more detailed study is required to fully understand the dynamics of the accelerated cometary ions, looking at the flow pattern of accelerated ions as function of position relative to the comet and likely also as function of the magnetic field and implied upstream electric field direction.

The fluxes of ions recorded by RPC-ICA increase by about four orders of magnitude from initial/late observations and up to the period around perihelion. This is more than the change in insolation and ionization frequency (about one order of magnitude) and comet activity (about two orders of magnitude). For the accelerated cometary ions the explanation is likely, at least in part, geometrical. As activity increases, the flow of accelerated cometary ions becomes more antisunward, more fluid-like, and less along the local solar wind electric field direction. Therefore, the likelihood that *Rosetta* will be along the flight path of accelerated cometary ions increases, while the area over which the ions spread out decreases. For the lower energy ions, a part of the reason may be that as densities fall, the spacecraft becomes less negatively charged, or even positively charged. Thus, part of the lowest energy population can no longer be measured by RPC-ICA. One may however note that the measured fluxes of low energy ions ($<$50 eV) and accelerated cometary ions ($>$100 eV) varies in a very similar fashion over the mission, except for the decrease in accelerated cometary ion fluxes close to perihelion (Fig. 3). This is observed despite the fact that the cold cometary ion fluxes have been scaled to a reference altitude. The actual level of the flux is relatively constant, as was seen in Fig. 4. The similarity between the cold ion flux, scaled to 20 km altitude, and the accelerated ion flux, not scaled in any way, thus indicates that the accelerated ion flux is proportional to the total outflow. This is found despite the widely varying distance to the nucleus. This indicates that whereas we can see a variation in accelerated ion flux with nucleus distance, the flux varies more with comet activity.

Finally we note that there are some cases where a signal is seen over a large energy range at the end of the mission, appearing in 2016 May as *Rosetta* goes very close to the nucleus. The ions are seen moving more or less antisunward. This signal appears only

when *Rosetta* is close to the nucleus. The nature of the signal is yet to be determined. Comparison with the RPC-IES instrument indicates that the signal is not real as RPC-IES has at least on some occasions had a free field of view in the same direction and not detected any signal. At the same time, the signal appears triggered by certain external circumstances, like high local pressure.

4 CONCLUSIONS

We have shown an overview of data from the RPC-ICA instrument from arrival at comet 67P in 2014 August until end of mission on 2016 September 30. The behaviour of the mass loaded solar wind is described in more detail in Behar et al. (2017). Here, we note that the solar wind disappeared from the *Rosetta* location in 2015 April, to re-appear again in 2015 December. *Rosetta* thus moved from a mass-loaded solar wind into a solar wind cavity, where the solar wind magnetic field was still present. Cometary ions dominated the density throughout this period, with most density in a cold population with energy below a few 10 eV. The accelerated cometary ions at times reached densities of a few 100 cm^{-3}. The accelerated cometary ions had an antisunward flow and a cone angle less than 90° throughout the mission with the exception of a few events late in the mission. These late events will be the subject of further evaluation, but are currently suspected to be artefacts.

Around perihelion *Rosetta* was located in a region where the accelerated ion fluxes decreased, as did the maximum energy of the cometary ions. There is thus an inner region into which cometary ions accelerated further upstream and moving antisunward are less likely to be observed, in agreement with previous observations (Mandt et al. 2016). We suggest that the inner region with less energetic ions may form due to the flow pattern of the accelerated cometary ions, i.e. the ions flow around the obstacle of the denser inner region, or through the effect of charge exchange collisions. Model work will have to show if there may be enough charge exchange collisions outside the location of *Rosetta* and whether these would give the observed change of the energy spectra. Both explanations are consistent with the somewhat higher fluxes of accelerated cometary ions further away from the comet nucleus in the dayside region, despite the general antisunward flow.

Whereas *Rosetta* was located in a number of different regions of the cometary environment, from mass-loaded solar wind via solar wind cavity to the region with less accelerated cometary ions and sometimes into (likely extensions of) the diamagnetic cavity, the sampling of different spatial regions of the comet magnetosphere was still very limited. Therefore, numerical models will be very important to fully understand the spatial structure of the comet environment.

ACKNOWLEDGEMENTS

Rosetta is a European Space Agency (ESA) mission with contributions from its member states and the National Aeronautics and Space Administration (NASA). *Rosetta*'s Philae lander is provided by a consortium led by DLR, MPS, CNES and ASI. The work on RPC-ICA was funded by the Swedish National Space Board under contracts 108/12,112/13, 96/15, 94/11 and by the Swedish Research Council under contract 2015-04187. Work at the Royal Belgian Institute for Space Aeronomy was supported by the Belgian Science Policy Office through the Solar-Terrestrial Centre of Excellence and by PRODEX/ROSETTA/ROSINA PEA 4000107705. Work at University of Oslo is supported by the Research Council of Norway grant no. 240000. Work at Imperial College London is supported by STFC of UK under grants ST/K001051/1 and ST/N000692/1. We acknowledge the staff of CDDP and IC for the use of AMDA and the RPC Quicklook data base (provided by a collaboration between the Centre de Données de la Physique des Plasmas (CDPP) supported by CNRS, CNES, Observatoire de Paris and Université Paul Sabatier, Toulouse and Imperial College London, supported by the UK Science and Technology Facilities Council). The raw RPC-ICA data are available through the PSA archive of ESA and a calibrated data set will be made available. We are indebted to the whole *Rosetta* mission team, Science Ground Segment and *Rosetta* Mission Operation Control for their hard work making this mission possible.

REFERENCES

Behar E., Nilsson H., Wieser G. S., Nemeth Z., Broiles T. W., Richter I., 2016a, Geophys. Res. Lett., 43, 1411
Behar E., Lindkvist J., Nilsson H., Holmström M., Stenberg-Wieser G., Ramstad R., Götz C., 2016b, A&A, 596, A42
Behar E., Nilsson H., Alho M., Goetz C. C., Tsurutani B., 2017, MNRAS, this issue
Beth A. et al., 2016, MNRAS, 462, S562
Bieler A. et al., 2015, A&A, 583, A7
Broiles T. W. et al., 2015, A&A, 583, A21
Broiles T. W. et al., 2016a, J. Geophys. Res. (Space Phys.), 121, 7407
Broiles T. W. et al., 2016b, MNRAS, 462, S312
Burch J., Goldstein R., Cravens T., Gibson W., Lundin R., Pollock C., Winningham J., Young D., 2007, Space Sci. Rev., 128, 697
Burch J. L., Cravens T. E., Llera K., Goldstein R., Mokashi P., Tzou C.-Y., Broiles T., 2015, Geophys. Res. Lett., 42, 5125
Carr C. et al., 2007, Space Sci. Rev., 128, 629
Clark G. et al., 2015, A&A, 583, A24
Coates A. J., Johnstone A. D., Wilken B., Jockers K., Glassmeier K.-H., 1989, J. Geophys. Res., 94, 9983
Cravens T., Gombosi T., 2004, Adv. Space Res., 33, 1968
Edberg N. J. T. et al., 2015, Geophys. Res. Lett., 42, 4263
Edberg N. J. T. et al., 2016, MNRAS, 462, S45
Eriksson A. I. et al., 2007, Space. Sci. Rev., 128, 729
Eriksson A. I. et al., 2017, A&A, in press
Fuselier S. A. et al., 2015, A&A, 583, A2
Fuselier S. A. et al., 2016, MNRAS, 462, S67
Galand M. et al., 2016, MNRAS, 462, S331
Glassmeier K.-H., Boehnhardt H., Koschny D., Kührt E., Richter I., 2007, Space Sci. Rev., 128, 1
Goetz C. et al., 2016a, MNRAS, 462, S459
Goetz C. et al., 2016b, A&A, 588, A24
Goetz C., Volwerk M., Richter I., Glassmeier K.-H., 2017, MNRAS, 469, S268
Goldstein R. et al., 2015, Geophys. Res. Lett., 42, 3093
Gunell H. et al., 2017, A&A, 600, A3
Hansen K. C. et al., 2016, MNRAS, 462, S491
Hässig M. et al., 2015, Science, 347, aaa0276
Henri P. et al., 2017, MNRAS, in press
Johnstone A. D. et al., 1993, A&A, 273
Karlsson T. et al., 2017, Geophys. Res. Lett., 44, 1641
Krankowsky D. et al., 1986, Nature, 321, 326
Lundin R. et al., 2006, Icarus, 182, 308
Luspay-Kuti A. et al., 2015, A&A, 583, A4
Madanian H. et al., 2016, J. Geophys. Res. (Space Phys.), 121, 5815
Mandt K. E. et al., 2016, MNRAS, 462, S9
Martinecz C. et al., 2008, Planet. Space Sci., 56, 780
Mendis D. A., Houpis H. L. F., Marconi M. L., 1985, Fundam. Cosm. Phys., 10, 2
Nemeth Z. et al., 2016, MNRAS, 462, S415
Neugebauer M., 1990, Rev. Geophys., 28, 231

Nicolaou G., Behar E., Nilsson H., Wieser M., Yamauchi M., Bercic L., Stenberg Wieser G., 2017, MNRAS, this issue
Nilsson H. et al., 2007, Space Sci. Rev., 128, 671
Nilsson H. et al., 2015a, Science, 347, aaa0571
Nilsson H. et al., 2015b, A&A, 583, A20
Odelstad E. et al., 2015, Geophys. Res. Lett., 42, 10, 126
Odelstad E., Eriksson A. I., Stenberg Wieser G., 2017, MNRAS, this issue
Rème H., 1991, Wash. DC Am. Geophys. Union Geophys. Monogr. Ser., 61, 87
Richardson I. G., Cowley S. W. H., Hynds R. J., Tranquille C., Sanderson T. R., Wenzel K.-P., 1987, Planet. Space Sci., 35, 1323
Richter I. et al., 2015, Ann. Geophys., 33, 1031
Simon Wedlund C. et al., 2016, A&A, 587, A154
Simon Wedlund C. et al., 2017, A&A, in press
Stenberg Wieser G., Odelstad E., Nilsson H., Wieser M., 2017, MNRAS, this issue
Szegö K. et al., 2000, Space Sci. Rev., 94, 429
Vigren E., Eriksson A., 2017, AJ, 153, 150
Yang L., Paulsson J. J. P., Simon Wedlund C., Odelstad E., Edberg N. J. T., Koenders C., Eriksson A. I., Miloch W. J., 2016, MNRAS, 462, S33
Young D. T. et al., 2004, Icarus, 167, 80

This paper has been typeset from a TEX/LATEX file prepared by the author.